



1 **Parametrizations of size distribution and refractive index of biomass burning organic**
2 **aerosol with black carbon content**

3 **Biao Luo^{1,2}, Ye Kuang^{1,2,*}, Shan Huang^{1,2,*}, Qicong Song^{1,2}, Weiwei Hu³, Wei Li^{1,2}, Yuwen Peng^{1,2},**
4 **Duohong Chen⁴, Dingli Yue⁴, Bin Yuan^{1,2}, Min Shao^{1,2}**

5 ¹ Institute for Environmental and Climate Research, Jinan University, Guangzhou, China.

6 ² Guangdong-Hongkong-Macau Joint Laboratory of Collaborative Innovation for Environmental
7 Quality, Guangzhou, China.

8 ³ State Key Laboratory of Organic Geochemistry and Guangdong Key Laboratory of Environmental
9 Protection and Resources Utilization, Guangzhou Institute of Geochemistry, Chinese Academy of
10 Sciences, Guangzhou 510640, China

11 ⁴ Guangdong Ecological and Environmental Monitoring Center, State Environmental Protection Key
12 Laboratory of Regional Air Quality Monitoring, Guangzhou 510308, China

13 Corresponding author: Ye Kuang (kuangye@jnu.edu.cn) and Shan Huang

14 (shanhuang_eci@jnu.edu.cn)

15

16

17

18

19

20



21 Abstract

22 Biomass burning organic aerosol (BBOA) impacts significantly on climate and regional air
23 quality directly through scattering and absorbing solar radiation and indirectly through acting as
24 cloud condensation nuclei. However, fundamental parameters in the simulation of BBOA radiative
25 effects and cloud activities such as size distribution and refractive index remain poorly
26 parameterized in models. In this study, biomass burning events were frequently observed during
27 autumn in the Pearl River Delta region, China. Aerosol physical properties including aerosol size
28 distributions, aerosol scattering coefficients and aerosol absorptions as well as aerosol chemical
29 compositions were comprehensively measured during these biomass burning events. An improved
30 absorption Ångström exponent (AAE) ratio method considering both variations and spectral
31 dependence of black carbon AAE was proposed to differentiate brown carbon (BrC) absorptions
32 from total aerosol absorptions. BBOA size distributions, mass scattering and absorption efficiency
33 were retrieved based on the changes in aerosol number size distributions, scattering coefficients and
34 derived BrC absorptions that occurred with BBOA spikes. Geometric mean diameter of BBOA
35 volume size distribution D_{gv} depended largely on combustion conditions, ranging from 245 to 505
36 nm, and a linear relationship between D_{gv} and $\Delta BC/\Delta BBOA$ was achieved. Retrieved BBOA mass
37 scattering efficiency, ranges from 3 to 7.5 m²/g, depending nonlinearly on D_{gv} (R=0.86) which was
38 confirmed by Mie theory simulations. Retrieved real part of BBOA refractive index ranges from
39 1.47 to 1.64, with evidences showing that its variations might depend largely on combustion
40 efficiency, which however requires further comprehensive investigations. Retrieved BBOA mass
41 absorption efficiencies and imaginary parts of BBOA refractive index ($m_{i,BBOA}$) correlated highly
42 with $\Delta BC/\Delta BBOA$ (R>0.88), but changes almost linearly with $\Delta BC/\Delta BBOA$ (R>0.88) which differs
43 much with previous findings. Consistent with results of previous studies, the variations of $m_{i,BBOA}$
44 as a function of optical wavelength λ can be well parameterized using $m_{i,BBOA}(\lambda) =$
45 $m_{i,BBOA}(520) \times (\frac{\lambda}{520})^{w_{BBOA}}$. The spectral dependence parameter w_{BBOA} ranged from 2.5 to 5.5 with
46 an average of 4.7 which is in generally higher than w_{BBOA} values predicted by previous
47 parameterization schemes, however, is actually consistent with previous laboratory results of similar
48 $\Delta BC/\Delta BBOA$ ranges. In addition, w_{BBOA} is also generally linearly correlated (R=-0.51) with
49 $\Delta BC/\Delta BBOA$. These findings have significant implications for simulating BBOA climate effects



50 and suggest that linking both BBOA refractive index and BBOA volume size distributions to black
51 carbon content might be a feasible and a good choice for climate models.

52

53

54

55

56

57

58 **1 Introduction**

59 Biomass burning organic aerosol (BBOA) emitted from natural and anthropogenic fire activities,
60 represents a major fraction of atmospheric primary organic aerosols, impacts significantly on climate
61 and regional air quality directly through scattering and absorbing solar radiation and indirectly through
62 acting as cloud condensation nuclei (Saleh et al., 2014; Saleh et al., 2015; Wang et al., 2016a; Zhang et
63 al., 2020; Liu et al., 2020b). BBOA size distributions are crucial for simulating aerosol-cloud
64 interactions, and BBOA scattering plays significant role in direct aerosol cooling effects and local
65 visibility degradation. BBOA is also a major contributor to atmospheric brown carbon (BrC) on a
66 global scale (Wang et al., 2016a) because of its non-negligible light absorption contribution in the near-
67 ultraviolet to visible wavelength. Accurate representation of BBOA size distributions, scattering and
68 absorption in climate models are crucial for BBOA radiative forcing simulations, and bias in biomass
69 burning absorption representation in models can result in biomass burning radiative forcing range from
70 cooling to warming (Brown et al., 2021). BBOA size distribution and refractive index are fundamental
71 parameters in the simulation of BBOA radiative effects and cloud activities, however, remain poorly
72 parameterized in models. Currently, our comprehensive knowledge of BBOA optical and physical
73 properties were primarily obtained from laboratory measurements (Janhäll et al., 2010; Saleh et al.,
74 2013; McClure et al., 2020). Although field measurements of biomass burning events were reported by
75 many studies (Laskin et al., 2015), however, only a few of them focused simultaneously on both BBOA
76 size distributions and optical properties (Reid et al., 2005b; Reid et al., 2005a; Laing et al., 2016), and
77 their parameterizations were reported by few studies. Comprehensive field measurements and
78 simultaneous characterization of BBOA size distributions, scattering and absorption properties and



79 retrieval of real and imaginary part of BBOA refractive index as well as their parameterizations remain
80 lacking, hindering the accurate representation of BBOA size distributions and refractive index in
81 climate models.

82 In-situ field measured aerosols are mixtures of different aerosol components emitted from
83 different sources and formed through different pathways. The BBOA mass concentrations might be
84 identified through source apportionment of organic aerosols using positive matrix factorization (PMF)
85 technique on the basis of aerosol mass spectrometer measurements (Kuang et al., 2021a). However,
86 the BBOA size distributions, BBOA scattering properties and BBOA light absorptions are usually quite
87 difficult to separate from properties of the entire aerosol populations. As a result, BBOA physical
88 properties such as size distribution, mass scattering efficiency (MSE), mass absorption efficiency
89 (MAE) and refractive index of biomass burning aerosols characterized in in-situ field measurements
90 are usually not specific to BBOA (Laing et al., 2016). Especially, parameterization of the imaginary
91 part of the BBOA refractive index ($m_{i,BBOA}$) have received wide attentions in recent years due to its
92 critical role in BBOA absorptivity representation in climate models (Saleh, 2020b). However, the yet
93 available parameterization schemes were primarily based on laboratory experiments, with very few
94 field measurements based results available (Lu et al., 2015). Liu et al. (2021) observed the evolution
95 of $m_{i,BBOA}$ in a real atmospheric environment chamber for different fire conditions at hourly scales
96 after emission under different oxidation conditions. Still, the spectral dependence parameterization of
97 $m_{i,BBOA}$ on the basis of in-situ field measurements covering a wavelength range from ultraviolet to
98 near-infrared remain lacking.

99 The key reason limiting the on-line characterization of BBOA refractive index based on the real
100 atmosphere measurements is that the on-line accurate quantification of BrC light absorption has been
101 a challenge due to the entanglement of black carbon (BC) absorption. Many studies have shown that
102 the distinct difference between BC and BrC spectral absorption characteristics represented by
103 Ångström law can be used to segregate BrC absorptions from measured total aerosol absorptions by
104 assuming a constant absorption Ångström exponent (AAE) of BC (AAE_{BC}) (de Sa et al., 2019; Wang
105 et al., 2016b; Yang et al., 2009). The BrC absorption retrieval accuracy of this constant AAE method
106 depends highly on the representativeness of used AAE_{BC} . Results of field and laboratory studies
107 demonstrated that AAE_{BC} varies under different pollution and emission conditions (Zhang et al.,
108 2019a; Laskin et al., 2015). Model simulations and field observations show that AAE_{BC} is affected by



109 many factors such as BC mixing state, morphology, BC mass size distribution as well as optical
110 wavelength, and values of AAE_{BC} can reach up to 1.6 for specific wavelength pairs (Lack and Cappa,
111 2010). Recent studies have modified the AAE method through a better consideration of AAE_{BC}
112 variations. Zhang et al. (2019b) used the $AAE_{880-990}$ obtained from real-time aethalometer
113 measurements as AAE_{BC} , considering that aerosol absorptions at near infrared wavelengths are
114 associated only with BC. Other studies determined AAE_{BC} through Mie theory simulations using
115 constrained BC mass or BC mixing states as inputs (Li et al., 2019; Wang et al., 2018; Qin et al.,
116 2018; Wang et al., 2016b). Wang et al. (2018) found remarkable AAE_{BC} wavelength dependence and a
117 relatively stable ratio between AAE_{BC} of certain wavelength ranges, which could be used to represent
118 spectral dependence of AAE_{BC} . However, this ratio method proposed by Wang et al. (2018) assumes
119 that BrC absorption contributes negligibly at 520 nm, which might bring some uncertainties and cannot
120 be used to retrieve the spectral characterization of BrC absorption for wavelengths near and beyond
121 520 nm.

122 In this study, aerosol chemical compositions, size distributions as well as aerosol scattering and
123 absorption coefficients were measured at a rural site in the Pearl River Delta (PRD) region of China,
124 where biomass burning events frequently occurred in autumn and played significant roles in regional
125 air quality (Liu et al., 2014). An improved method considering both variations and spectral dependence
126 of AAE_{BC} was proposed to quantify the BrC absorption spectral dependence from 370 nm to 660 nm.
127 The differential method was applied to biomass burning events to estimate BBOA scattering and
128 absorption properties as well as BBOA size distributions. The combination of identified BBOA size
129 distributions, MSE and MAE were used to retrieve the real and imaginary parts of BBOA refractive
130 index using the Mie theory, based on which parameterizations of BBOA size distributions and
131 refractive index using BC/BBOA ratio were investigated.

132 **2 Materials and methods**

133 **2.1 Field measurements.**

134 Field measurements were performed from 30 September to 17 November 2019 at a rural site in
135 Heshan county, Guangdong Province, China. The site locates at the top of a small hill surrounded by
136 small villages and residential towns, and usually experiences air masses from cities of the highly
137 industrialized PRD region. This site is authorized as a supersite operated by the provincial



138 environmental monitoring authority, therefore continuous qualified measurements of meteorological
139 parameters such as air temperature, relative humidity (RH), wind speed and direction, and pollutant
140 measurements are carried out. Physical and chemical properties of ambient aerosol were
141 comprehensively measured during this field campaign, including multi-wavelength aerosol scattering
142 coefficients measurement under nearly dry ($RH < 30\%$) and controlled but fixed RH conditions using
143 humidified nephelometer system (Kuang et al., 2019; Kuang et al., 2021b), multi-wavelength absorption
144 measurements using an aethalometer (Magee, AE33 (Drinovec et al., 2015)), aerosol size distribution
145 measurements using a scanning mobility particle sizer (SMPS, TSI 3080) and an aerodynamic particle
146 sizer (APS; TSI Inc., Model 3321), and aerosol chemical composition measurements using an soot-
147 particle aerosol mass spectrometer, etc. The AE33 measurements were only valid from 30 September
148 to 31 October. Continuous and stable measurements of aerosol chemical composition using the aerosol
149 mass spectrometer measurements were valid since 10 October. More details on the site and instrument
150 set up can be found in Kuang et al. (2021b).

151 Accurate AAE and absorption measurements are crucial for the BrC quantification. Results of
152 previous comparison studies of aerosol absorption measurements between AE33 and photoacoustic
153 soot spectrometer demonstrated that AAE will only be slightly influenced by the particle collection of
154 AE33 on the filter (Saleh et al., 2013; Zhao et al., 2020). As to the absorption corrections associated
155 with loading effect and multiple scattering effect caused by filter collection. Dual-spot mode was
156 applied in AE33 measurements for dealing with aethalometer loading effect. A Multiple-scattering
157 correction factor (C) was used to convert measured attenuation coefficient (b_{ATN}) by AE33 to the
158 absorption coefficient of ambient aerosols (b_{abs}) at each wavelength through $b_{abs} = b_{ATN}/C$. C is
159 considered to be dependent on filter tape, however, results of previous studied have reported that C
160 might also varies with aerosol chemical compositions (Wu et al., 2009; Collaud Coen et al., 2010). The
161 filter tape 8060 was used for AE33 during this field campaign. Zhao et al. (2020) evaluated C of filter
162 tape 8060 through comparing AE33 measurements with a three-wavelength photoacoustic soot
163 spectrometer, and their results demonstrated that C is almost independent of wavelength and differs
164 little among measurements of different locations. Thus the wavelength independent C of filter tape
165 8060 of 2.9 recommended by Zhao et al. (2020) was used, and this value is also almost the median
166 value of C ranges used in Kasthuriarachchi et al. (2020).



167 **2.2 Aerosol mass spectrometer measurements.**

168 The size-resolved aerosol chemical compositions of dried aerosol particles with aerodynamic
169 diameter less than 1 μm were measured using a soot particle aerosol mass spectrometer (SP-AMS,
170 Aerodyne Research, Inc., Billerica, MA, USA)(Kuang et al., 2021b). The mass concentrations of
171 aerosol chemical compositions from SP-AMS were validated by offline $\text{PM}_{2.5}$ filter measurements,
172 SMPS aerosol volume concentration measurements and online measurements for inorganic aerosol
173 components. More details on SP-AMS data quality assurance can be found in Kuang et al. (2021b).
174 The source identification of organic aerosols was conducted using positive matrix factorization (PMF)
175 method based on the high-resolution OA data collected in V-mode (only tungsten vaporizer). Six-
176 factors were identified based on the best performance criteria of PMF quality parameters. Two primary
177 OA factors include biomass burning organic aerosols (BBOA, $\text{O/C}=0.48$) and a hydrocarbon-like
178 organic aerosols (HOA, containing cooking emissions, $\text{O/C}=0.02$). The other four factors were
179 associated with secondary formations or aging processes: 1) more oxygenated organic aerosols
180 (MOOA, $\text{O/C}=1$, associated with regional airmass(Kuang et al., 2021b)), 2) less oxygenated organic
181 aerosols (LOOA, $\text{O/C}=0.72$, related to daytime photochemical formation), 3) nighttime-formed
182 organic aerosols (Night-OA, $\text{O/C}=0.32$, highly correlated with Nitrate with $r=0.67$, and exhibited sharp
183 increases during the evening), and 4) aged BBOA (aBBOA, $\text{O/C}=0.39$, exhibited similar diurnal
184 behavior with LOOA with strong daytime production). The mass spectral profile and time series of
185 these organic aerosol factors were shown in Fig.S3, and these factors were partly discussed in Kuang
186 et al. (2021b). The BBOA factor will be the focus of this study. On the basis of the scheme proposed
187 by Kuwata et al. (2012), the density of BBOA (ρ_{BBOA}) and HOA was estimated as 1.25 and 1.15 g/cm^3
188 with O:C and H:C as inputs, and used in this study.

189

190 **2.3 Quantification of BrC absorptions based on the light absorption wavelength dependence**
191 **measurements.**

192 BrC absorbs significantly at near-UV and short-visible wavelengths but exhibits strong
193 wavelength dependence (Saleh, 2020a). The deconvolution of the spectral dependence of measured
194 aerosol light absorption has been a common method to retrieve the BrC and black carbon (BC)
195 absorption distribution:

196
$$\sigma_{\text{BrC}}(\lambda) = \sigma_a(\lambda) - \sigma_{\text{BC}}(\lambda) \quad (1)$$



197 Where $\sigma_a(\lambda)$ represents measured total aerosol absorption at wavelength λ , $\sigma_{BC}(\lambda)$ the absorption
198 associated with BC (includes influences of BC size distributions and mixing states, etc.), and $\sigma_{BrC}(\lambda)$
199 the light absorption contributed by BrC. The spectral dependence of BC absorption was usually
200 accounted for using the Angstrom exponent (AAE) law (Laskin et al., 2015), which describes BC
201 absorption as $\sigma_{BC}(\lambda) = K\lambda^{-AAE}$ where K is a constant factor associated with BC mass concentration.
202 The traditional method usually assumes a constant AAE of 1 (de Sa et al., 2019), or a wavelength
203 independent AAE derived from near infrared absorption measurements by assuming that the BrC
204 absorption is negligible at near infrared wavelengths. For example, $\sigma_{BC}(880\text{ nm})$ and $\sigma_{BC}(950\text{ nm})$
205 measured by AE33 can be used to formulate the spectral dependence of aerosol absorptions associated
206 with BC as the following:

$$207 \sigma_{BC}(\lambda) = \sigma_{BC}(880\text{ nm}) \times \left(\frac{880}{\lambda}\right)^{AAE_{BC,\lambda-880}} \quad (2)$$

$$208 AAE_{BC,\lambda-880} = AAE_{BC,950-880} \quad (3)$$

209 However, several recent modelling studies using Mie-theory and BC measurements demonstrated
210 that AAE_{BC} varies as a function of wavelength, and the wavelength independent assumption of AAE_{BC}
211 will bring large uncertainties into BrC calculation (Li et al., 2019; Wang et al., 2018). Wang et al. (2018)
212 found $AAE_{BC,520-880}$ and $AAE_{BC,370-520}$ differed much from each other, however, the
213 $AAE_{BC,370-520}/AAE_{BC,520-880}$ ratio varied little, and thus proposed an AAE ratio method to obtain
214 real-time $AAE_{BC,370-520}$ and further deduced $\sigma_{BC}(370\text{ nm})$. This method assumes that BrC
215 contributes negligibly at 520 nm, which might introduce uncertainties. In addition, this method is not
216 applicable in retrieving the spectral dependence of BrC absorption because only the ratio
217 $AAE_{BC,370-520}/AAE_{BC,520-880}$ was used. This modified wavelength-dependent AAE differentiation
218 method was further partially adopted by Li et al. (2019), using $AAE_{BC,370-520}$ to account for spectral
219 dependence of BC absorption for wavelengths < 520 nm and $AAE_{BC,520-880}$ for wavelengths > 520 nm,
220 thus the wavelength-dependent AAE_{BC} was partially but not thoroughly considered.

221 Considering the advantages of both methods of Wang et al. (2018) and Li et al. (2019), an
222 improved AAE ratio method was proposed to comprehensively tackle the spectral dependence of BC
223 absorption and also take real-time measured $AAE_{BC,950-880}$ into account, which combines the
224 modelled ratio $R_{AAE} = AAE_{BC,\lambda-880} / AAE_{BC,950-880}$ and measured $AAE_{BC,950-880}$ to derive
225 $AAE_{BC,\lambda-880}$ and further retrieve $\sigma_{BrC}(\lambda)$ with the combination of Eq.1 and Eq.2. The modelling



226 method of $AAE_{BC,\lambda-880}$ is consistent with Li et al. (2019) and more details are available in Supplement
227 Sect. S1. The wavelength dependence of AAE_{BC} are influenced by many factors such as BC refractive
228 index, coating shell refractive index as well as BC mixing state, and BC mass size distributions (Li et
229 al., 2019). A sensitivity experiment following the method of Li et al. (2019) is initiated to explore
230 impacts of these optical and mixing state parameters on $AAE_{BC,\lambda-880}$ and the ratio
231 $AAE_{BC,\lambda-880}/AAE_{BC,950-880}$. These parameters including the real part of the refractive index of BC
232 coating materials and BC-free particles (Real_NBC), real and imaginary parts of refractive index of
233 the BC core (Real_BC and Imag_BC), the mass fraction of externally mixed BC (r_{ext}), the number
234 fraction of BC-free particles (R_NBC), geometric standard deviation (GSD) and geometric mean
235 diameter (GM) of BC mass size distributions. Note that the imaginary parts of the refractive index of
236 BC particle coating materials and BC-free particles were not perturbed in these simulations and treated
237 as zero under the assumption of materials other than BC is non-absorbing. In order to separate effects
238 of BC and BrC on $AAE_{\lambda-880}$ changes, this assumption must be made to obtain $AAE_{BC,\lambda-880}$ variations
239 associated only with BC absorption changes. The defect of this method is that the entangling effects
240 of BrC coating on BC particles in $AAE_{BC,\lambda-880}$ variations are not considered. The results of
241 $AAE_{BC,370-880}$ is shown in Fig.1a. It shows that variations of both refractive index of BC and coating
242 materials as well as BC mixing states have non-negligible influences on $AAE_{BC,370-880}$, however the
243 BC mass size distributions represented by geometric standard deviation (GSD) and geometric mean
244 diameter (GM) of BC mass size distribution play the most important roles. Nevertheless, for results of
245 $AAE_{BC,\lambda-880} / AAE_{BC,950-880}$ shown in Fig.1b, when fixing the BC mass size distribution,
246 $AAE_{BC,\lambda-880}/AAE_{BC,950-880}$ exhibited much smaller variations, even the refractive index of BC and
247 shell or mixing state varied within atmospherically relevant ranges. The result of sensitive studies
248 shown in Fig.1b further confirmed the applicability of the proposed new AAE ratio method under
249 constrained BC mass size distributions. The elemental carbon fragments (Cx) retrieved from SP-AMS
250 measurements cannot be used to quantify BC mass concentrations due to the lack of calibration
251 parameters, however, its size distributions generally represent the relative contributions of BC mass
252 within different diameter ranges. The real-time measured normalized Cx distributions are therefore
253 used to distribute total BC mass to different diameter bins to calculate the ratio

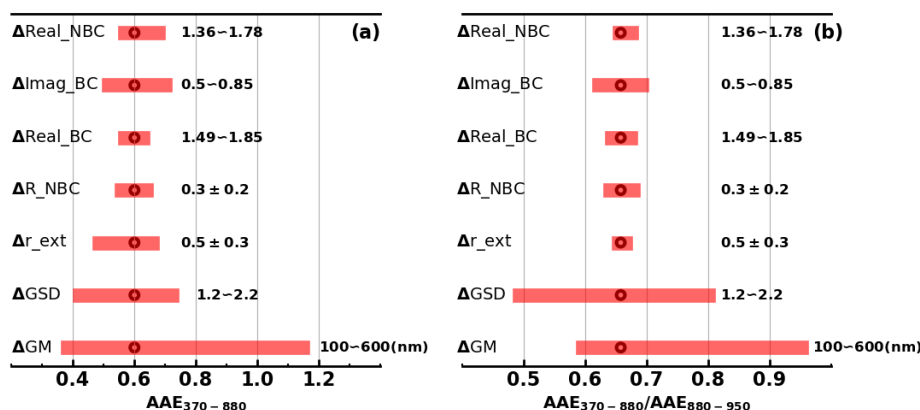


Figure 1. Changes in (a) $AAE_{BC,370-880}$ and (b) $AAE_{BC,370-880}/AAE_{BC,950-880}$ associated perturbations of different parameters.

254 $AAE_{BC,\lambda-880}/AAE_{BC,950-880}$, and the average normalized Cx distribution is shown in Fig.S4. The
 255 average AAE ratios of $AAE_{BC,370-880} / AAE_{BC,950-880}$, $AAE_{BC,470-880} / AAE_{BC,520-880}$,
 256 $AAE_{BC,590-880} / AAE_{BC,950-880}$, $AAE_{BC,660-880} / AAE_{BC,950-880}$, $AAE_{BC,370-880} / AAE_{BC,950-880}$ are
 257 0.79, 0.85, 0.88, 0.9 and 0.93 respectively. Based on this method, the spectral dependence of BrC
 258 absorption can be derived as the following:

$$259 \sigma_{BrC}(\lambda) = \sigma_a(\lambda) - \sigma_{BC}(880 \text{ nm}) \times \left(\frac{880}{\lambda}\right)^{AAE_{BC,950-880} \times R(\lambda)} \quad (4)$$

260 With this method, the effects of BrC coating on BC can still not be avoided, but the consideration of
 261 aerosol absorptions associated only with BC would be improved than before.

262 3 Results and discussions

263 3.1 Dominant contribution of BBOA to BrC absorption

264 Biomass burning plumes around the observation site were frequently observed during this field
 265 campaign at dusk as shown in Fig.S5(a,d) and only sometimes during daytime periods (Fig.S5(b, c)).
 266 The average diurnal variations of resolved primary OA factors including both BBOA and HOA are
 267 presented in Fig.S6, in which both average diurnal profiles of BBOA and HOA exhibited sharp
 268 increases around 18:00 local time (LT), which should be associated with frequently observed biomass
 269 burning events and supper cooking in villages and towns near this site. However, diurnal behaviors of
 270 BBOA and HOA differ much from about 06:00 LT to 16:00 LT. HOA exhibited continuous decreases
 271 during this daytime period, which was associated with boundary layer processes and re-partitioning



272 due to increasing temperature. The BBOA showed almost continuous but slow increases since morning
273 to the afternoon, indicating strong daytime emissions of BBOA as shown in Fig.S5(b, c), although not
274 as prominent as the BBOA emission just before the fall of nighttime. The probability distribution of
275 the ratio BBOA/HOA is also shown in Fig.S6b, which shows that the ratio BBOA/HOA reached
276 beyond 2 in 57% conditions with an average of 3.3, which demonstrates that biomass burning was a
277 dominant primary aerosol emission source during this field campaign.

278 The observed Angstrom Exponents between different wavelengths and 880 nm of total aerosol
279 absorption are shown in Fig.2a, the average values of $AAE_{370-880}$, $AAE_{470-880}$, $AAE_{520-880}$, $AAE_{590-880}$,
280 $AAE_{660-880}$, $AAE_{950-880}$ are 1.17, 1.23, 1.18, 1.15, 1.08, 1.04. The scatter plots of $AAE_{370-880}$ and the
281 ratio BBOA/BC shown in Fig.2b shows that $AAE_{370-880}$ was highly correlated with BBOA/BC ($r=0.8$),
282 indicating strong influences of BBOA on aerosol absorption wavelength dependence. The BrC
283 absorption at multiple wavelengths are extracted using the improved AAE ratio method introduced in
284 Sect.2, and statistical ranges of BrC absorption as well as their contributions to total aerosol absorption
285 are shown in Fig.2d. Average values of derived σ_{BrC} at 370 nm, 470 nm, 520 nm, 590 nm, 660 nm are
286 $19.1 Mm^{-1}$, $11.5 Mm^{-1}$, $6.4 Mm^{-1}$, $3.45 Mm^{-1}$, $1.13 Mm^{-1}$ and their contributions to total aerosol
287 absorption are 23%, 18%, 12%, 8%, 3% respectively. Similar to some previous studies (Tao et al.,
288 2020;Qin et al., 2018), these results shows that the contributions of BrC to aerosol absorption at
289 wavelengths of less than 590 nm are not negligible. The derived timeseries of $\sigma_{BrC,370}$ are shown in
290 Fig.S7d, depicting BBOA varying quite consistently with $\sigma_{BrC,370}$ and with high correlations
291 (correlation coefficients between σ_{BrC} at 370 nm, 470 nm, 520 nm, 590 nm, 660 nm and BBOA
292 reaching 0.9, 0.83, 0.8, 0.76, 0.69), suggesting that BBOA was the dominant contributor to BrC
293 absorption.

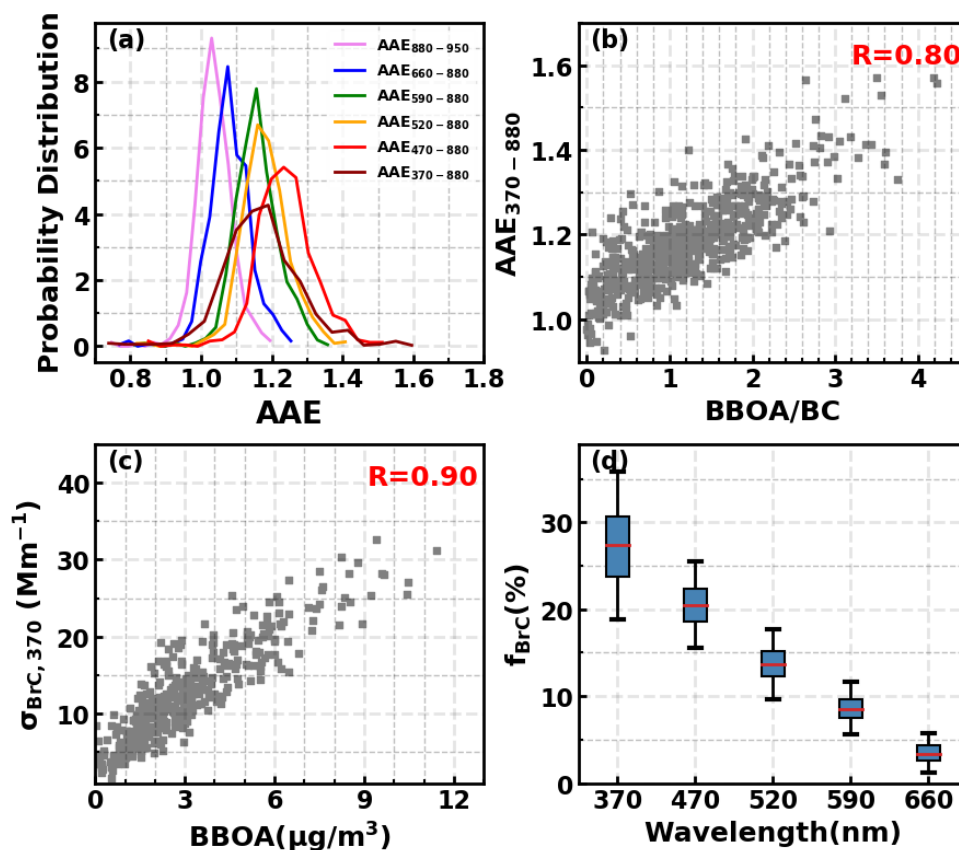


Figure 2. (a) Probability distribution of AAE between different wavelengths and 880 nm; (b) Correlations between AAE₃₇₀₋₈₈₀ and mass ratio of BBOA and BC; (c) Correlations between the BrC absorption coefficients at 370nm and the BBOA mass loadings; (d) Box-and-whisker plots of BrC absorption fractions at different wavelengths.

294

295 3.2 Identification of BBOA size distributions and their parameterizations

296 During the observation period, BBOA contributed dominantly to BrC absorptions and notable
297 biomass burning events represented by BBOA mass concentration spikes as shown in Fig.S7
298 frequently occurred. These biomass burning spikes are related with biomass burning plumes that swept
299 over the observation site, thus the difference between aerosol properties measured before and during
300 these spikes can represent the properties of biomass burning aerosols. These spikes usually occurred
301 during supper cooking time (~ 18:00 LT) and typical bio-fuels used for cooking are mainly vegetation



302 fuels such as local woods. SMPS directly measures the aerosol particle number size distribution
303 (PNSD), thus also providing particle volume size distribution measurements (PVSD). Fig.3a shows
304 the average differences of mass concentrations of different aerosol components of identified spikes
305 with simultaneous valid SMPS data. Ammonium nitrate (AN) and ammonium sulfate (AS) were
306 determined as the dominant form of ammonium, sulfate and nitrate ions during this field campaign
307 and paired using the scheme proposed by Gysel et al. (2007). It shows that inorganic aerosol
308 components increased a little bit, which is consistent with previous studies (Hecobian et al., 2011; Pratt
309 et al., 2011) that biomass burning emits tiny amounts of inorganic aerosol. However, it is difficult to
310 quantify how much of these inorganic aerosol increases was attributed to biomass burning emissions
311 because the biomass burning spikes were usually observed during the periods with secondary nitrate
312 formation (Kuang et al., 2021a). Secondary organic aerosol components changed a little, with the slight
313 increase of aBBOA suggesting plumes were aged a little bit. Obvious increases of HOA were observed,
314 but the most prominent increase was BBOA. The average $\Delta BC/\Delta BBOA$ ratio for cases when BC
315 measurements were valid was 0.22, suggesting the observed biomass burning events are likely flaming
316 burning conditions with high combustion efficiency (Reid et al., 2005b; McClure et al., 2020). The
317 cooking related organic aerosol could not be separated from HOA in PMF analysis. The co-increase
318 of HOA are due to the fact that these identified spikes occurred during periods of supper cooking as
319 discussed before.

320 The average aerosol particle number and volume size distribution differences (Δ PNSD and Δ
321 PVSD) calculated as the PNSD and PVSD differences between those at the BBOA peak concentration
322 and those before the BBOA spikes are shown in Fig.3b, the example of calculating Δ PNSD and Δ
323 PVSD is shown in Fig.S8. The average Δ PVSD can be well fitted using two lognormal modes (Mode
324 1 and Mode 2), the dominant one is BBOA and another is mostly associated with HOA according to
325 the aerosol mass changes. Geometric mean (D_{gv}) and standard deviation (σ_g) values of the two PVSD
326 lognormal modes are 180, 390 and 1.46, 1.5, respectively. In addition, the SP-AMS measurements

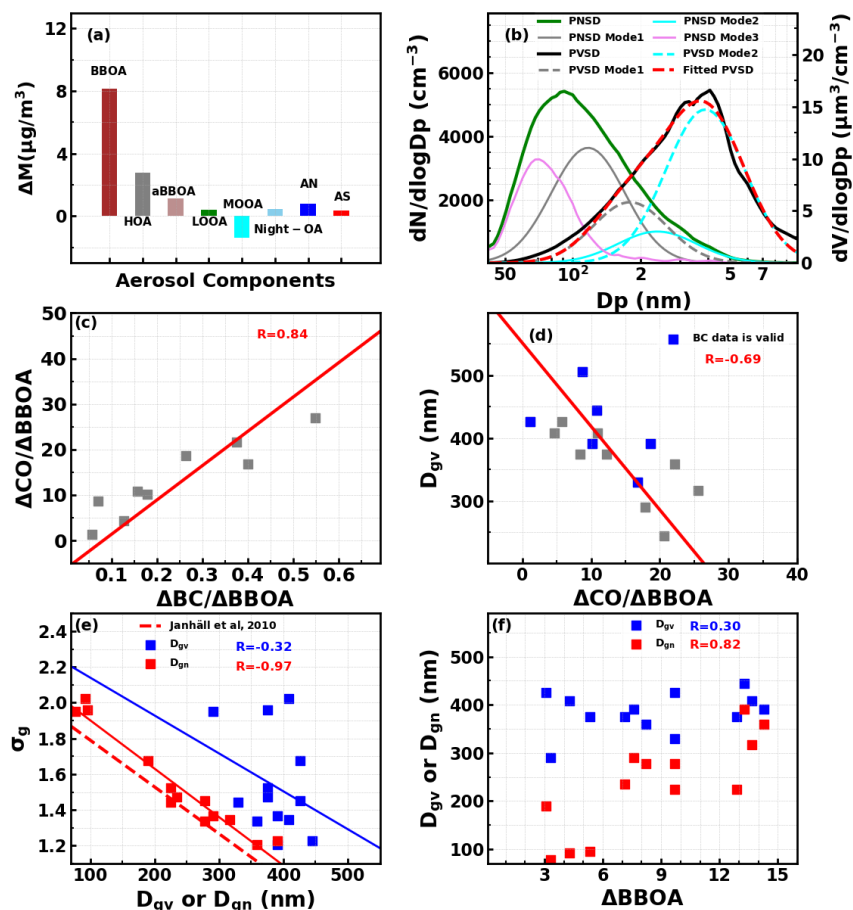


Figure 3. (a) Average differences of aerosol components before and end of BBOA spikes; (b) Corresponding particle average number and volume size distribution difference (ΔPNSD and ΔPVSD); (c) Relationship between $\Delta\text{CO}/\Delta\text{BBOA}$ and $\Delta\text{BC}/\Delta\text{BBOA}$; (d) The relationships between identified D_{gv} of BBOA spikes and corresponding $\Delta\text{CO}/\Delta\text{BBOA}$ ($\text{ppb}/(\mu\text{g}/\text{m}^3)$); (e) relationship between retrieved D_{gv} and σ_g , as well as D_{gv} and σ_g . (f) relationships between D_{gv} or D_{gn} and ΔBBOA .

327 provides organic aerosol size distributions with vacuum aerodynamic diameter (D_a), their average
 328 distribution difference of organic aerosols during these spikes are also shown in Fig.S9 and could be
 329 generally well fitted using two lognormal modes of BBOA and HOA. The $D_{gv,Da}$ and σ_g values of the
 330 identified modes were 175, 395 and 1.46, 1.55, respectively. D_{va} and mobility diameter D_p of the
 331 SMPS were related through the effective density of particles as $\rho_e = D_a/(D_m \times C)$, where ρ_e is the
 332 aerosol effective density and C a factor related to aerosol shape, for which a value of 0.8 was adopted
 333 (Jayne et al., 2000). Based on densities of BBOA and HOA introduced in Sect.2.2, identified D_{gv} of
 334 BBOA and HOA from SP-AMS measurements of 395 and 190 nm, which were quite close to the D_{gv}



335 identified from SMPS measurements, further confirming the results from SMPS measurements. The
336 average Δ PNSD is shown in Fig.3b, displaying a number concentrations peak near 90 nm, however,
337 influences of HOA need to be excluded to identify biomass burning PNSD modes. As shown in Fig.3b,
338 converting the identified BBOA and HOA Δ PVSD modes to Δ PNSD modes cannot explain the
339 observed PNSD difference, the remaining mode is lognormal and peaks at 70 nm. These results
340 indicate that two modes existed for biomass burning aerosols during this campaign, which is consistent
341 with findings of previous studies (Okoshi et al., 2014;Liu et al., 2020a).

342 For spikes where Δ BBOA dominated the mass changes, the D_{gv} and σ_g of BBOA PVSD was
343 retrieved by fitting the larger mode of Δ PVSD, with retrieved results shown in Fig.3c and Fig.3d. The
344 retrieved D_{gv} ranged from 245 nm to 505 nm with an average of 380 nm. Physicochemical properties
345 of biomass burning emissions depended largely on combustion conditions. BC/BBOA ratio is a proxy
346 of biomass combustion efficiencies (McClure et al., 2020), and it was found that Δ CO/ Δ BBOA was
347 highly correlated with Δ BC/ Δ BBOA (Fig.3c, $R=0.84$). Thus, Δ CO/ Δ BBOA was also used as a proxy
348 for combustion efficiency in this study. Higher Δ CO/ Δ BBOA corresponds to higher combustion
349 efficiency. Retrieved D_{gv} values were moderately but negatively correlated with Δ CO/ Δ BBOA ($R=-$
350 0.69), and a linear relationship $D_{gv}=551-13.3\times\Delta$ CO/ Δ BBOA was derived. This result is qualitatively
351 consistent with previous studies that biomass burning aerosols were mainly in the accumulation mode
352 and their average sizes generally decreased as the combustion efficiency increases (Reid and Hobbs,
353 1998;Janhäll et al., 2010). Retrieved σ_g ranges from 1.2 to 2.0 with an average of 1.5, and is negatively
354 and weakly correlated with D_{gv} ($R=-0.32$). Reid et al. (2005b) reported that D_{gv} is typically in the range
355 of 250 to 300 nm with the σ_g on the order of 1.6 to 1.9 for freshly generated smoke, and 30-80 nm
356 larger for aged smoke with smaller σ_g (1.4 to 1.6). Levin et al. (2010) performed laboratory
357 combustion of various wildland fuels, and reported D_{gv} of 200 to 570 nm and σ_g of 1.68 to 2.97. The
358 average D_{gv} and σ_g is near the reported D_{gv} range by Reid et al. (2005b) for aged smoke. Geometric
359 mean of PNSD (D_{gn}) values are converted from retrieved D_{gv} and σ_g and also shown in Fig.3e. D_{gn}
360 ranges from 88 to 391 nm with an average of 235 nm. The average D_{gn} is similar with the reported
361 average D_{gn} of aged smoke but the range even beyond the range (100-300 nm) for both fresh and aged
362 smokes reported by Janhäll et al. (2010) in which literature published D_{gn} are reviewed, and also
363 beyond the range (about 130-240 nm) reported in Laing et al. (2016) for aged biomass burning aerosol



364 from wildfires in Siberia and the Western USA. Similar with results of Janhäll et al. (2010), σ_g is highly
365 but negatively correlated with D_{gn} ($R=-0.97$). The derived linear relationship $\sigma_g=2.17-0.0027 \times D_{gn}$ is
366 close to that reported in Janhäll et al. (2010) (Fig.3e). Janhäll et al. (2010) defined the fresh smoke as
367 plumes younger than 1 h, but aged smoke are mostly plumes older than one day. The aged smoke in
368 Laing et al. (2016) were also transported over 4-10 days. However, the smoke plumes reported in this
369 study occurred during supper cooking time, and swept over the observation site last about 1-3h (from
370 the beginning to BBOA concentration fall back the background levels) which are consistent the time
371 need for cooking, which means that the age of plumes are on the order of hour and near freshly
372 emitted. This is indirectly confirmed by the observed changes in particle number concentrations that
373 small aitken mode dominate the particle number concentrations (Fig.3b), because coagulation is quick and
374 should cause a significant decrease in number concentrations of Aitken mode aerosols in times scales
375 of hours (Sakamoto et al., 2015; Laing et al., 2016; Sakamoto et al., 2016). These results demonstrate
376 that D_{gn} and D_{gv} varies over a wide range for near freshly emitted BBOA from vegetation fire smokes.
377 Laing et al. (2016) reported that D_{gn} was highly correlated with plume aerosol mass concentrations
378 (PM), but not with any normalized variable such as $\Delta PM/\Delta CO$. Similar results were obtained in this
379 study (Fig.3f). The derived D_{gn} was weakly correlated ($R=-0.21$) with $\Delta CO/\Delta BBOA$, but highly
380 correlated with $\Delta BBOA$ ($R=0.82$). The new finding here is that D_{gv} correlated obviously with
381 $\Delta CO/\Delta BBOA$, but weakly with $\Delta BBOA$. As discussed in implications, BBOA volume size
382 distributions determine BBOA bulk optical properties thus accurate representations of BBOA volume
383 size distributions in climate models might be more important than accurate representations of BBOA
384 number size distributions.

385

386 3.3 BBOA Mass Scattering Efficiency and retrieval of the real part of BBOA refractive index

387 The measured aerosol scattering coefficients at 525 nm ($\sigma_{sp,525}$) during BBOA spikes were used
388 to calculate the MSEs using the differential method, thereby retrieving the real part of BBOA refractive
389 index (m_R) on the basis of Mie theory. Truncation error, non-ideality of light source and RH conditions
390 need to be corrected in the calculation of $\sigma_{sp,525}$ values under dry condition. The truncation error and
391 non-ideality of light source was corrected using the empirical formula provided by Qiu et al. (2021).
392 RH_0 in the dry nephelometer was in the range of 20% to 45% with an average of 31%, and corrected



393 by considering measured aerosol optical hygroscopicity through $\sigma_{sp,525} = \sigma_{sp,525,measured} / (1 + \kappa_{sca} \times$
394 $\frac{RH_0}{100 - RH_0})$, where κ_{sca} is the optical hygroscopicity parameter derived from aerosol light scattering
395 enhancement factor measurements (Kuang et al., 2017). To quantify MSE_{BBOA} , MSEs of other aerosol
396 components are needed. Using the paired campaign average size distributions of AS and AN (Fig.S1),
397 MSEs of AS and AN was calculated as 4.6 and 4.8 m^2/g , which were identical with those identified by
398 Tao et al. (2019) during autumn at an urban area in this region, but much higher than average values
399 reported in Hand and Malm (2007). Through the analysis of the OA distribution measured by SP-AMS,
400 it was found that the size distribution of SOA can be represented by two lognormal modes (Fig.S2).
401 One is aBBOA, and the other one includes MOOA, Night-OA, and MOOA. Thus, MSE of MOOA,
402 Night-OA, LOOA (MSE_{SOA}) was determined to be 6.3 m^2/g , and MSE_{aBBOA} was 4.5 m^2/g . MSE_{HOA}
403 was calculated to be 3.2 m^2/g using the size distribution identified in Fig.3b. MSE_{BC} was calculated as
404 2.8 m^2/g using the average normalized Cx fragments distributions, which was also very close to the
405 MSE of elemental carbon determined by Tao et al. (2019) (2.6 m^2/g). The changes of aerosol scattering
406 coefficients associated only with BBOA can be calculated as $\Delta\sigma_{sp,BBOA} = \Delta\sigma_{sp,measured} - \Delta AS \times$
407 $MSE_{AS} - \Delta AN \times MSE_{AN} - \Delta HOA \times MSE_{HOA} - \Delta BC \times MSE_{BC} - \Delta aBBOA \times MSE_{aBBOA} - (\Delta Night-$
408 $OA + \Delta MOOA + \Delta LOOA) \times MSE_{SOA}$. More details about MSE calculations of these components can be
409 found in Sect.S1. In addition, to minimize the influences of uncertainties of used MSEs of other aerosol
410 components on MSE_{BBOA} derivations, only spikes with sum changes of ΔAS , ΔAN , $\Delta Night-OA$,
411 $\Delta MOOA$, $\Delta LOOA$ and $\Delta aBBOA$ accounting for less than 25% of $\Delta BBOA$ were used. Average changes
412 of aerosol components for these spikes are shown in Fig.4a, with changes of most individual aerosol
413 components being almost negligible.

414 As shown in Fig.4b, the derived $\Delta\sigma_{sp,525}$ associated with BBOA was highly correlated with Δ
415 BBOA ($R=0.91$). MSE_{BBOA} ranged from 3.1 to 7.5 m^2/g with an average of 5.3 m^2/g . Reid et al. (2005a)
416 reviewed the MSEs of biomass burning (MSE_{BB}) aerosols and reported a range of 3.2-4.2 m^2/g for
417 temperate and boreal fresh smoke, and larger for corresponding aged smoke (4.3 m^2/g). McMeeking
418 et al. (2005) theoretically calculated the MSEs of smoke-influenced aerosols and reported a MSE range
419 of 3-6 m^2/g . Levin et al. (2010) conducted MSE_{BB} measurements of fresh biomass burning smokes of
420 various fuel types, reported a MSE_{BB} range of 1.6 to 5.7 m^2/g . Laing et al. (2016) reported a MSE_{BB}
421 range of 2.5 to 4.7 for aged biomass burning aerosols of wildfires, and similar range was reported by

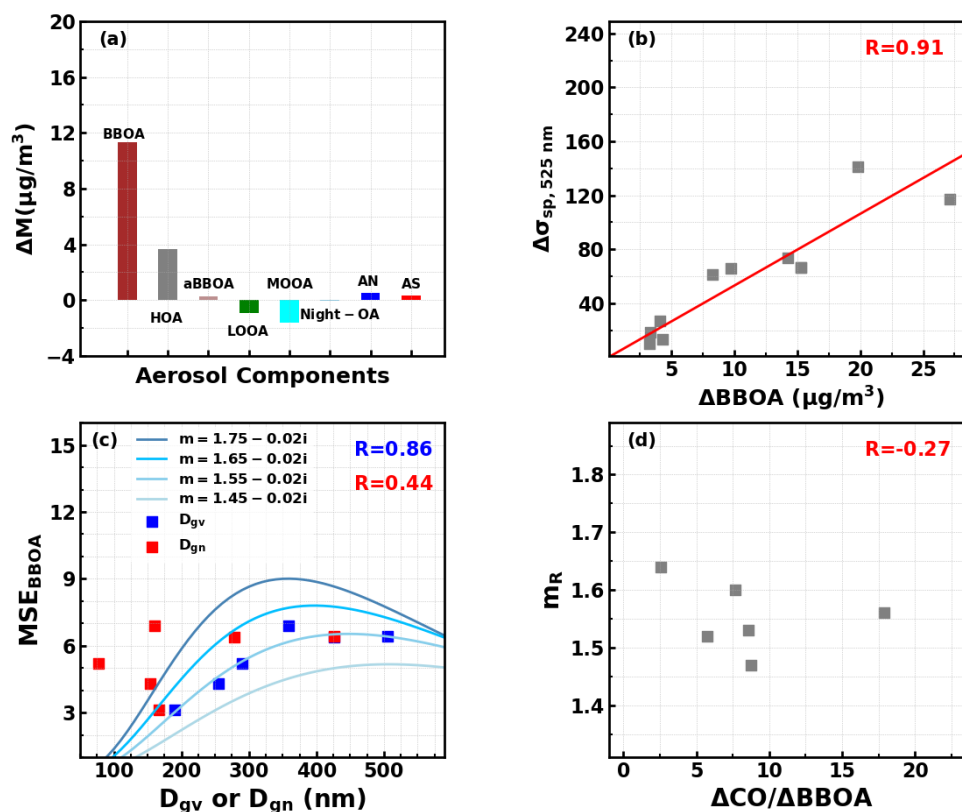


Figure 4. (a) Average differences of aerosol components between nearest background and the peak of BBOA spikes; (b) Relationships between derived $\Delta\sigma_{sp}$ at 525 nm only associated with BBOA and ΔBBOA ; (c) Relationships between retrieved MSE_{BBOA} and D_{gn} or D_{gv} ; (d) Relationship between retrieved m_R and $\Delta\text{CO}/\Delta\text{BBOA}$.

422 Briggs et al. (2017). However, no study has specifically investigated MSE_{BBOA} variations, which are
 423 very crucial for biomass burning aerosol climate effects simulations, since aerosol components in
 424 models are usually separately represented (Riemer et al., 2019). Although organic aerosols usually
 425 dominate mass concentration of biomass burning aerosols, the reported MSE_{BBOA} range is generally
 426 higher than previously reported MSE_{BB} ranges, which are likely associated with the fact that MSE_{BB}
 427 includes influences of low scattering efficiency components such as BC. Another reason for this is that
 428 the identified geometric mean size of BBOA in this study was generally larger than those reported
 429 before. Many studies have shown that aerosol size distribution have crucial impacts on MSE
 430 variations (Hand and Malm, 2007). Both results of Levin et al. (2010) and Laing et al. (2016) have
 431 reported that MSE_{BB} of biomass burning aerosols were highly correlated with D_{gn} . The relationship



432 between MSE_{BBOA} and D_{gn} as well as D_{gv} were investigated (Fig.4c, only six points with both D_{gv} and
433 σ_g retrieval are available). Unlike results of previous studies, MSE_{BBOA} were positively but weakly
434 correlated with D_{gn} ($R=0.44$). However, MSE_{BBOA} were highly correlated to D_{gv} ($R=0.86$), and
435 exhibited non-linear response with the increase of D_{gv} . The non-linear increase phenomenon was
436 reported first but confirmed by Mie theory simulations by assuming a fixed σ_g of 1.5 under varying
437 conditions of D_{gv} and refractive index (Fig.4c).

438 Aerosol refractive index was a fundamental parameter in simulating aerosol optical properties in
439 models. However, aerosol refractive index investigations specific to BBOA is scarce because the direct
440 retrieval of aerosol refractive index at least needs accurate and simultaneous representations of
441 MSE_{BBOA} , BBOA density and BBOA size distribution shape. Only few studies have indirectly
442 retrieved m_R of biomass burning related aerosols. For example, McMeeking et al. (2005) and Levin et
443 al. (2010) have retrieved m_R of biomass burning or smoke-influenced aerosols through using an
444 iterative algorithm to match measured size distributions of different principles (mobility-related size
445 versus optical size), reported m_R ranges were 1.56 to 1.59 and 1.41 to 1.61, respectively. In this study,
446 m_R values of BBOA were retrieved using Mie theory with MSE_{BBOA} , D_{gn} , σ_g and BBOA density as
447 inputs as introduced in Sect.1.3 of the supplement. Note that the retrieval of m_R would also be affected
448 by the imaginary part of BBOA refractive index ($m_{i,BBOA}$), and the $m_{i,BBOA}$ parameterization as a
449 function of $\Delta CO/\Delta BBOA$ introduced in the next section was used. Retrieved m_R ranges from 1.47 to
450 1.64 with an average of 1.56. If m_R changes from 1.47 to 1.64 can result in a double MSE_{BBOA} for
451 given BBOA size distributions. Thus, reported $m_{R,BBOA}$ range was wide with respect to MSE
452 simulations and needs to be carefully parameterized in climate modes. BBOA refractive index is
453 determined by its chemical structure thus its variation might be associated with fire combustion
454 conditions. The relationship between $m_{R,BBOA}$ and $\Delta CO/\Delta BBOA$ was further investigated and shown
455 in Fig.4d. For $\Delta CO/\Delta BBOA$ below $10 \text{ ppb}/\mu\text{g} \cdot \text{m}^3$, m_R was negatively correlated with $\Delta CO/\Delta BBOA$
456 ($R=-0.71$) thus like $\Delta BC/\Delta BBOA$, which however, was not as significant ($R=-0.27$). These results
457 demonstrate that fire combustion conditions might have significant impacts on $m_{R,BBOA}$, however,
458 needs further investigation.

459

460 **3.4 BBOA mass absorption efficiency and parameterizations of the spectral dependence of**
461 **imaginary part of BBOA refractive index**

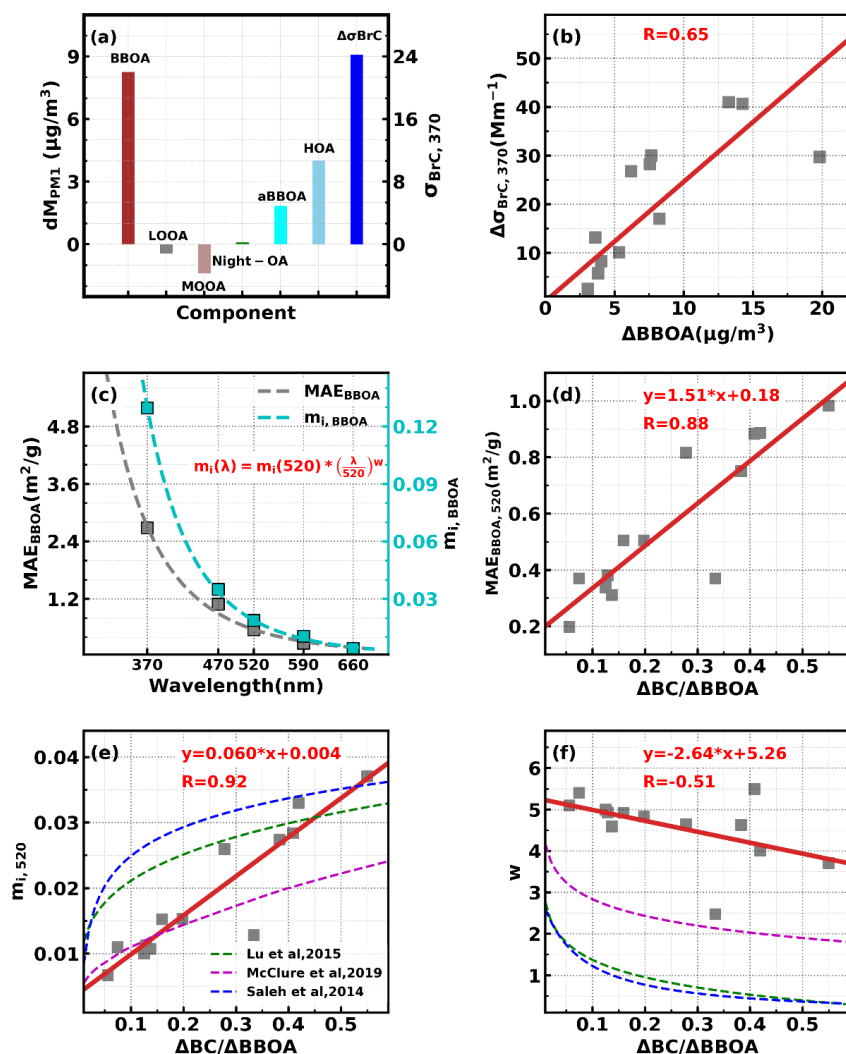


Figure 5. (a) Average changes of organic aerosol components for BBOA spikes when BC measurements are available; (b) Relationships between derived $\Delta\sigma_{BrC}$ at 525 nm only associated with BBOA and Δ BBOA; (c) Average spectral dependence of MAE_{BBOA} and BBOA m_i ; (d) Relationship between MAE_{BBOA} at 525 nm and Δ CO/ Δ BBOA; (e) Relationship between BBOA m_i at 525 nm and Δ CO/ Δ BBOA; (f) Relationship between the spectral dependence parameter w of BBOA m_i and Δ CO/ Δ BBOA.

462 Derived BrC absorptions of BBOA spikes were used to calculate MAE_{BBOA} and retrieve
 463 imaginary part of BBOA refractive index ($m_{i,BBOA}$) in combination of retrieved BBOA size
 464 distributions using Mie theory. Average changes of organic aerosol components for spikes with



465 available σ_{BrC} values are shown in Fig.5a. Δ BBOA dominated the mass changes, however, non-
466 negligible changes for aBBOA, HOA and MOOA. The average MAE_{HOA}, MAE_{aBBOA} and MAE_{MOOA}
467 are estimated using multilinear regression for all data points with values at 370 nm of 0.1, 0.96 and 0.9
468 m²/g, respectively. Thus the $\Delta\sigma_{BrC,BBOA}$ can be derived as $\Delta\sigma_{BrC,BBOA}(\lambda)=\Delta\sigma_{BrC,derived}-\Delta$ HOA \times
469 MAE_{HOA}(λ)- Δ aBBOA \times MAE_{aBBOA}(λ)- Δ MOOA \times MSE_{MOOA}(λ). As shown in Fig.5b, $\Delta\sigma_{BrC,BBOA}$
470 was moderately correlated with Δ BBOA (R=0.65), suggesting significant changes of MAE_{BBOA}.
471 Derived MAE_{BBOA} exhibited strong wavelength dependence and average values at wavelengths of 370,
472 470, 520, 590, and 660 nm were 2.46,0.99,0.53,0.28, 0.11 m²/g, respectively. Fig.5c shows the spectral
473 dependence of MAE_{BBOA} and retrieved $m_{i,BBOA}$, and formula form that parameterize the spectral
474 dependence was consistent with previous studies (Saleh et al., 2014). BBOA absorption properties
475 depended largely on combustion conditions, both MAE_{BBOA} and retrieved m_i at 520 nm was highly
476 and linearly correlated with Δ BC/ Δ BBOA (Fig.5d and Fig.5e). Results regarding $m_{i,BBOA}$
477 parameterizations as a function of Δ BC/ Δ BBOA of previous studies are also shown in Fig.5e. Results
478 of Saleh et al. (2014) and Lu et al. (2015) at 550 nm were higher for Δ BC/ Δ BBOA in the range of 0.05
479 to 0.4. Curve of McClure et al. (2020) well described the $m_{i,BBOA}$ variations for Δ BC/ Δ BBOA less than
480 0.2. The $m_{i,BBOA}$ spectral dependence parameter w_{BBOA} ranged from 2.5 to 5.5 with an average of 4.7,
481 was linearly and negatively correlated to Δ BC/ Δ BBOA and much higher than those reported in Saleh
482 et al. (2014) and Lu et al. (2015). The w_{BBOA} was also higher than the fitted line of McClure et al.
483 (2020), however, was actually consistent with the w_{BBOA} range reported in Fig.5c of McClure et al.
484 (2020) for a BC/OA range of 0.1 to 0.55.

485

486 **4. Implications for simulating climate effects of BBOA**

487 Findings of BBOA size distributions, real and imaginary parts of BBOA refractive index in this
488 study have important implications for climate modelling of BBOA radiative effects. The volume
489 dominant mode of biomass burning aerosols contribute dominantly to aerosol mass, which are most
490 important for BBOA scattering and absorption properties. The volume dominant mode also contributed
491 dominantly to number concentration for diameter range of >150 nm, and this diameter range played
492 the dominant role in BBOA aerosols as cloud condensation nuclei (Chen et al., 2019). However,
493 previous studies usually parameterized number geometric mean diameter D_{gn} as a function of



494 combustion conditions. It was found that BBOA mass scattering efficiency correlated well with the
495 volume geometric mean diameter D_{gv} , but correlated poorly with D_{gn} , which was in contradiction with
496 previous results (Levin et al., 2010; Laing et al., 2016) that BBOA mass scattering efficiency was highly
497 correlated with D_{gn} . However, the simulation results shown in Fig.S10 explained the contrast, that
498 aerosol scattering efficiency were very sensitive to σ_g changes for fixed D_{gn} , however, are much less
499 sensitive to σ_g changes for D_{gv} , and retrieved σ_g varied over a wide range from 1.2 to 2 in this study.
500 In addition, it was found that D_{gn} correlated poorly with normalized parameters such as $\Delta CO/\Delta BBOA$,
501 whereas D_{gv} correlated highly with $\Delta CO/\Delta BBOA$. Therefore, representing BBOA volume size
502 distribution of the volume dominant mode as a function of combustion conditions in climate models
503 might be a better choice if using only one size distribution mode (Stier et al., 2005; Dentener et al.,
504 2006), however needs further and synthesized research on this topic. In view of this, on the basis of
505 the relationships between $\Delta CO/\Delta BBOA$ and $\Delta BC/\Delta BBOA$, the D_{gv} were parameterized as $D_{gv}=632-$
506 $1000 \times \Delta BC/\Delta BBOA$, and might be applicable in climate models (Saleh, 2020b).

507 The real part of BBOA refractive $m_{R,BBOA}$ was fundamental parameter for simulating BBOA
508 scattering properties in Climate models, however, a constant was usually used due to the lack of
509 adequate parameterizations (Brown et al., 2021). Significant changes were found in $m_{R,BBOA}$ in this
510 study (1.47 to 1.64), and the variations were likely closely associated with changes in fire combustion
511 conditions represented by $\Delta CO/\Delta BBOA$. For BBOA refractive index, the imaginary part ($m_{i,BBOA}$) are
512 currently recommended to be parameterized as a function of BC/BBOA ratio (Saleh et al., 2014), which
513 is supported by results of several studies (Lu et al., 2015; McClure et al., 2020). Results of this study
514 suggests that it might be also feasible to parameterize $m_{i,BBOA}$ as a function of BC/BBOA, however,
515 needs further comprehensive investigations.

516 The imaginary part of BBOA refractive index, $m_{i,BBOA}$, plays crucial role in representing BBOA
517 absorptivity in climate models. Linear relationships between $m_{i,BBOA}$ as well as the spectral dependence
518 parameter w and BC/OA are reported for the first time in this study. The observed BC/OA ratio (0.05
519 to 0.55) locates within the upper range of previously reported BC/OA values. Few measurements
520 regarding aerosol refractive index and size-distributions are available in this BC/OA range, and no
521 researches have focused on parameterizations of BBOA refractive index in this specific BC/OA range,
522 thus results of this study have partially filled this gap. Results of McClure et al. (2020) demonstrate
523 that a sigmoidal curve fits well the $m_{i,BBOA}$ variations for a wide range of BC/OA ratio (10^{-5} to 10),



524 however the $m_{i,BBOA}$ variations are not well captured by the fitted curve for $BC/OA > 0.1$. We
525 recommend for more sophisticated parameterizations of $m_{i,BBOA}$ under different BC/OA ranges.

526

527

528 **Data availability.** The data used in this study are available from the corresponding author upon request
529 Ye Kuang (kuangye@jnu.edu.cn) and Shan Huang (shanhuang_eci@jnu.edu.cn)

530 **Competing interests.** The authors declare that they have no conflict of interest.

531

532 **Author Contributions.**

533 YK and SH designed this experiment, YK conceived and led this research. BL and YK wrote the
534 manuscript. SH lead the SP-AMS measurements and particle number size distribution measurements.
535 SH performed the PMF analysis and Cx fragment analysis, revised the manuscript. MS and BY planned
536 this campaign. DC and DY provided authority of conducting the campaign in Heshan supersite and
537 gave data availability from the site. All other coauthors have contributed to this paper in different ways.

538 **Acknowledgments**

539 This work is supported by the National Natural Science Foundation of China (grant No. 41805109,
540 41807302), National Key Research and Development Program of China (grant No. 2017YFC0212803,
541 2016YFC0202206), Key-Area Research and Development Program of Guangdong Province (grant No.
542 2019B110206001), Special Fund Project for Science and Technology Innovation Strategy of
543 Guangdong Province (grant No.2019B121205004), Guangdong Natural Science Funds for
544 Distinguished Young Scholar (grant No. 2018B030306037) and Guangdong Innovative and
545 Entrepreneurial Research Team Program (grant No. 2016ZT06N263).

546

547

548

549

550

551 **References**

552 Briggs, N. L., Jaffe, D. A., Gao, H., Hee, J. R., Baylon, P. M., Zhang, Q., Zhou, S., Collier, S. C., Sampson, P. D., and Cary, R. A.:



- 553 Particulate Matter, Ozone, and Nitrogen Species in Aged Wildfire Plumes Observed at the Mount Bachelor Observatory,
554 *Aerosol and Air Quality Research*, 16, 3075-3087, 10.4209/aaqr.2016.03.0120, 2017.
- 555 Brown, H., Liu, X., Pokhrel, R., Murphy, S., Lu, Z., Saleh, R., Mielonen, T., Kokkola, H., Bergman, T., Myhre, G., Skeie, R. B.,
556 Watson-Paris, D., Stier, P., Johnson, B., Bellouin, N., Schulz, M., Vakkari, V., Beukes, J. P., van Zyl, P. G., Liu, S., and Chand,
557 D.: Biomass burning aerosols in most climate models are too absorbing, *Nature communications*, 12, 277,
558 10.1038/s41467-020-20482-9, 2021.
- 559 Chen, L., Li, Q., Wu, D., Sun, H., Wei, Y., Ding, X., Chen, H., Cheng, T., and Chen, J.: Size distribution and chemical
560 composition of primary particles emitted during open biomass burning processes: Impacts on cloud condensation nuclei
561 activation, *Science of The Total Environment*, 674, 179-188, <https://doi.org/10.1016/j.scitotenv.2019.03.419>, 2019.
- 562 Collaud Coen, M., Weingartner, E., Apituley, A., Ceburnis, D., Fierz-Schmidhauser, R., Flentje, H., Henzing, J. S., Jennings,
563 S. G., Moerman, M., Petzold, A., Schmid, O., and Baltensperger, U.: Minimizing light absorption measurement artifacts of
564 the Aethalometer: evaluation of five correction algorithms, *Atmos. Meas. Tech.*, 3, 457-474, 10.5194/amt-3-457-2010,
565 2010.
- 566 de Sa, S. S., Rizzo, L. V., Palm, B. B., Campuzano-Jost, P., Day, D. A., Yee, L. D., Wernis, R., Isaacman-VanWertz, G., Brito, J.,
567 Carbone, S., Liu, Y. J. J., Sedlacek, A., Springston, S., Goldstein, A. H., Barbosa, H. M. J., Alexander, M. L., Artaxo, P., Jimenez,
568 J. L., and Martin, S. T.: Contributions of biomass-burning, urban, and biogenic emissions to the concentrations and light-
569 absorbing properties of particulate matter in central Amazonia during the dry season, *Atmospheric Chemistry and Physics*,
570 19, 7973-8001, 10.5194/acp-19-7973-2019, 2019.
- 571 Dentener, F., Kinne, S., Bond, T., Boucher, O., Cofala, J., Generoso, S., Ginoux, P., Gong, S., Hoelzemann, J. J., Ito, A., Marelli,
572 L., Penner, J. E., Putaud, J. P., Textor, C., Schulz, M., van der Werf, G. R., and Wilson, J.: Emissions of primary aerosol and
573 precursor gases in the years 2000 and 1750 prescribed data-sets for AeroCom, *Atmos. Chem. Phys.*, 6, 4321-4344,
574 10.5194/acp-6-4321-2006, 2006.
- 575 Drinovec, L., Mocnik, G., Zotter, P., Prevot, A. S. H., Ruckstuhl, C., Coz, E., Rupakheti, M., Sciare, J., Muller, T., Wiedensohler,
576 A., and Hansen, A. D. A.: The "dual-spot" Aethalometer: an improved measurement of aerosol black carbon with real-
577 time loading compensation, *Atmospheric Measurement Techniques*, 8, 1965-1979, 10.5194/amt-8-1965-2015, 2015.
- 578 Gysel, M., Crosier, J., Topping, D. O., Whitehead, J. D., Bower, K. N., Cubison, M. J., Williams, P. I., Flynn, M. J., McFiggans,
579 G. B., and Coe, H.: Closure study between chemical composition and hygroscopic growth of aerosol particles during
580 TORCH2, *Atmos. Chem. Phys.*, 7, 6131-6144, 10.5194/acp-7-6131-2007, 2007.
- 581 Hand, J. L., and Malm, W. C.: Review of aerosol mass scattering efficiencies from ground-based measurements since 1990,
582 *Journal of Geophysical Research: Atmospheres*, 112, <https://doi.org/10.1029/2007JD008484>, 2007.
- 583 Hecobian, A., Liu, Z., Hennigan, C. J., Huey, L. G., Jimenez, J. L., Cubison, M. J., Vay, S., Diskin, G. S., Sachse, G. W., Wisthaler,
584 A., Mikoviny, T., Weinheimer, A. J., Liao, J., Knapp, D. J., Wennberg, P. O., Kürten, A., Crounse, J. D., Clair, J. S., Wang, Y., and
585 Weber, R. J.: Comparison of chemical characteristics of 495 biomass burning plumes intercepted by the NASA DC-8 aircraft
586 during the ARCTAS/CARB-2008 field campaign, *Atmos. Chem. Phys.*, 11, 13325-13337, 10.5194/acp-11-13325-2011, 2011.
- 587 Janhäll, S., Andreae, M. O., and Pöschl, U.: Biomass burning aerosol emissions from vegetation fires: particle number and
588 mass emission factors and size distributions, *Atmos. Chem. Phys.*, 10, 1427-1439, 10.5194/acp-10-1427-2010, 2010.
- 589 Jayne, J. T., Leard, D. C., Zhang, X., Davidovits, P., Smith, K. A., Kolb, C. E., and Worsnop, D. R.: Development of an Aerosol
590 Mass Spectrometer for Size and Composition Analysis of Submicron Particles, *Aerosol Science and Technology*, 33, 49-70,
591 10.1080/027868200410840, 2000.
- 592 Kasthuriarachchi, N. Y., Rivellini, L.-H., Adam, M. G., and Lee, A. K. Y.: Light Absorbing Properties of Primary and Secondary
593 Brown Carbon in a Tropical Urban Environment, *Environmental science & technology*, 54, 10808-10819,
594 10.1021/acs.est.0c02414, 2020.
- 595 Kuang, Y., Zhao, C., Tao, J., Bian, Y., Ma, N., and Zhao, G.: A novel method for deriving the aerosol hygroscopicity parameter
596 based only on measurements from a humidified nephelometer system, *Atmos. Chem. Phys.*, 17, 6651-6662, 10.5194/acp-



597 17-6651-2017, 2017.

598 Kuang, Y., He, Y., Xu, W., Sun, Y., Zhao, P., Cheng, Y., Zhao, G., Tao, J., Ma, N., Su, H., Zhang, Y., Sun, J., Cheng, P., Yang, W.,
599 Zhang, S., Wu, C., and Zhao, C.: Distinct diurnal variation of organic aerosol hygroscopicity and its relationship with
600 oxygenated organic aerosol, *Atmos. Chem. Phys. Discuss.*, 2019, 1-33, 10.5194/acp-2019-633, 2019.

601 Kuang, Y., Huang, S., Xue, B., Luo, B., Song, Q., Chen, W., Hu, W., Li, W., Zhao, P., Cai, M., Peng, Y., Qi, J., Li, T., Chen, D., Yue,
602 D., Yuan, B., and Shao, M.: Contrasting effects of secondary organic aerosol formations on organic aerosol hygroscopicity,
603 *Atmos. Chem. Phys. Discuss.*, 2021, 1-27, 10.5194/acp-2021-3, 2021a.

604 Kuang, Y., Huang, S., Xue, B. A., Luo, B. A., Song, Q. C., Chen, W., Hu, W. W., Li, W., Zhao, P. S., Cai, M. F., Peng, Y. W., Qi, J.
605 P., Li, T. G., Wang, S. H., Chen, D. H., Yue, D. L., Yuan, B., and Shao, M.: Contrasting effects of secondary organic aerosol
606 formations on organic aerosol hygroscopicity, *Atmospheric Chemistry and Physics*, 21, 10375-10391, 10.5194/acp-21-
607 10375-2021, 2021b.

608 Kuwata, M., Zorn, S. R., and Martin, S. T.: Using Elemental Ratios to Predict the Density of Organic Material Composed of
609 Carbon, Hydrogen, and Oxygen, *Environmental science & technology*, 46, 787-794, 10.1021/es202525q, 2012.

610 Lack, D. A., and Cappa, C. D.: Impact of brown and clear carbon on light absorption enhancement, single scatter albedo
611 and absorption wavelength dependence of black carbon, *Atmospheric Chemistry and Physics*, 10, 4207-4220,
612 10.5194/acp-10-4207-2010, 2010.

613 Laing, J. R., Jaffe, D. A., and Hee, J. R.: Physical and optical properties of aged biomass burning aerosol from wildfires in
614 Siberia and the Western USA at the Mt. Bachelor Observatory, *Atmos. Chem. Phys.*, 16, 15185-15197, 10.5194/acp-16-
615 15185-2016, 2016.

616 Laskin, A., Laskin, J., and Nizkorodov, S. A.: Chemistry of Atmospheric Brown Carbon, *Chemical Reviews*, 115, 4335-4382,
617 10.1021/cr5006167, 2015.

618 Levin, E. J. T., McMeeking, G. R., Carrico, C. M., Mack, L. E., Kreidenweis, S. M., Wold, C. E., Moosmüller, H., Arnott, W. P.,
619 Hao, W. M., Collett Jr, J. L., and Malm, W. C.: Biomass burning smoke aerosol properties measured during Fire Laboratory
620 at Missoula Experiments (FLAME), *Journal of Geophysical Research: Atmospheres*, 115,
621 <https://doi.org/10.1029/2009JD013601>, 2010.

622 Li, Z. J., Tan, H. B., Zheng, J., Liu, L., Qin, Y. M., Wang, N., Li, F., Li, Y. J., Cai, M. F., Ma, Y., and Chan, C. K.: Light absorption
623 properties and potential sources of particulate brown carbon in the Pearl River Delta region of China, *Atmospheric
624 Chemistry and Physics*, 19, 11669-11685, 10.5194/acp-19-11669-2019, 2019.

625 Liu, D. T., Li, S. Y., Hu, D. W., Kong, S. F., Cheng, Y., Wu, Y. Z., Ding, S., Hu, K., Zheng, S. R., Yan, Q., Zheng, H., Zhao, D. L.,
626 Tian, P., Ye, J. H., Huang, M. Y., and Ding, D. P.: Evolution of Aerosol Optical Properties from Wood Smoke in Real
627 Atmosphere Influenced by Burning Phase and Solar Radiation, *Environ. Sci. Technol.*, 55, 5677-5688,
628 10.1021/acs.est.0c07569, 2021.

629 Liu, J., Li, J., Zhang, Y., Liu, D., Ding, P., Shen, C., Shen, K., He, Q., Ding, X., Wang, X., Chen, D., Szidat, S., and Zhang, G.:
630 Source apportionment using radiocarbon and organic tracers for PM_{2.5} carbonaceous aerosols in Guangzhou, South
631 China: contrasting local- and regional-scale haze events, *Environmental science & technology*, 48, 12002-12011,
632 10.1021/es503102w, 2014.

633 Liu, J., Andersson, A., Zhong, G., Geng, X., Ding, P., Zhu, S., Cheng, Z., Zakaria, M. P., Bong, C. W., Li, J., Zheng, J., Zhang, G.,
634 and Gustafsson, Ö.: Isotope constraints of the strong influence of biomass burning to climate-forcing Black Carbon
635 aerosols over Southeast Asia, *Science of The Total Environment*, 744, 140359,
636 <https://doi.org/10.1016/j.scitotenv.2020.140359>, 2020a.

637 Liu, L., Cheng, Y., Wang, S., Wei, C., Pöhlker, M. L., Pöhlker, C., Artaxo, P., Shrivastava, M., Andreae, M. O., Pöschl, U., and
638 Su, H.: Impact of biomass burning aerosols on radiation, clouds, and precipitation over the Amazon: relative importance
639 of aerosol–cloud and aerosol–radiation interactions, *Atmos. Chem. Phys.*, 20, 13283-13301, 10.5194/acp-20-13283-2020,
640 2020b.



- 641 Lu, Z., Streets, D. G., Winijkul, E., Yan, F., Chen, Y., Bond, T. C., Feng, Y., Dubey, M. K., Liu, S., Pinto, J. P., and Carmichael, G.
642 R.: Light Absorption Properties and Radiative Effects of Primary Organic Aerosol Emissions, *Environmental science &*
643 *technology*, 49, 4868-4877, 10.1021/acs.est.5b00211, 2015.
- 644 McClure, C. D., Lim, C. Y., Hagan, D. H., Kroll, J. H., and Cappa, C. D.: Biomass-burning-derived particles from a wide variety
645 of fuels – Part 1: Properties of primary particles, *Atmos. Chem. Phys.*, 20, 1531-1547, 10.5194/acp-20-1531-2020, 2020.
- 646 McMeeking, G. R., Kreidenweis, S. M., Carrico, C. M., Lee, T., Collett Jr., J. L., and Malm, W. C.: Observations of smoke-
647 influenced aerosol during the Yosemite Aerosol Characterization Study: Size distributions and chemical composition,
648 *Journal of Geophysical Research: Atmospheres*, 110, <https://doi.org/10.1029/2004JD005389>, 2005.
- 649 Okoshi, R., Rasheed, A., Chen Reddy, G., McCrowey, C. J., and Curtis, D. B.: Size and mass distributions of ground-level sub-
650 micrometer biomass burning aerosol from small wildfires, *Atmospheric Environment*, 89, 392-402,
651 <https://doi.org/10.1016/j.atmosenv.2014.01.024>, 2014.
- 652 Pratt, K. A., Murphy, S. M., Subramanian, R., DeMott, P. J., Kok, G. L., Campos, T., Rogers, D. C., Prenni, A. J., Heymsfield,
653 A. J., Seinfeld, J. H., and Prather, K. A.: Flight-based chemical characterization of biomass burning aerosols within two
654 prescribed burn smoke plumes, *Atmos. Chem. Phys.*, 11, 12549-12565, 10.5194/acp-11-12549-2011, 2011.
- 655 Qin, Y. M., Tan, H. B., Li, Y. J., Li, Z. J., Schurman, M. I., Liu, L., Wu, C., and Chan, C. K.: Chemical characteristics of brown
656 carbon in atmospheric particles at a suburban site near Guangzhou, China, *Atmospheric Chemistry and Physics*, 18, 16409-
657 16418, 10.5194/acp-18-16409-2018, 2018.
- 658 Qiu, J., Tan, W., Zhao, G., Yu, Y., and Zhao, C.: New correction method for the scattering coefficient measurements of a
659 three-wavelength nephelometer, *Atmos. Meas. Tech.*, 14, 4879-4891, 10.5194/amt-14-4879-2021, 2021.
- 660 Reid, J. S., and Hobbs, P. V.: Physical and optical properties of young smoke from individual biomass fires in Brazil, *Journal*
661 *of Geophysical Research: Atmospheres*, 103, 32013-32030, <https://doi.org/10.1029/98JD00159>, 1998.
- 662 Reid, J. S., Eck, T. F., Christopher, S. A., Koppmann, R., Dubovik, O., Eleuterio, D. P., Holben, B. N., Reid, E. A., and Zhang, J.:
663 A review of biomass burning emissions part III: intensive optical properties of biomass burning particles, *Atmos. Chem.*
664 *Phys.*, 5, 827-849, 10.5194/acp-5-827-2005, 2005a.
- 665 Reid, J. S., Koppmann, R., Eck, T. F., and Eleuterio, D. P.: A review of biomass burning emissions part II: intensive physical
666 properties of biomass burning particles, *Atmos. Chem. Phys.*, 5, 799-825, 10.5194/acp-5-799-2005, 2005b.
- 667 Riemer, N., Ault, A. P., West, M., Craig, R. L., and Curtis, J. H.: Aerosol Mixing State: Measurements, Modeling, and Impacts,
668 *Reviews of Geophysics*, 57, 187-249, <https://doi.org/10.1029/2018RG000615>, 2019.
- 669 Sakamoto, K. M., Allan, J. D., Coe, H., Taylor, J. W., Duck, T. J., and Pierce, J. R.: Aged boreal biomass-burning aerosol size
670 distributions from BORTAS 2011, *Atmos. Chem. Phys.*, 15, 1633-1646, 10.5194/acp-15-1633-2015, 2015.
- 671 Sakamoto, K. M., Laing, J. R., Stevens, R. G., Jaffe, D. A., and Pierce, J. R.: The evolution of biomass-burning aerosol size
672 distributions due to coagulation: dependence on fire and meteorological details and parameterization, *Atmos. Chem.*
673 *Phys.*, 16, 7709-7724, 10.5194/acp-16-7709-2016, 2016.
- 674 Saleh, R., Hennigan, C. J., McMeeking, G. R., Chuang, W. K., Robinson, E. S., Coe, H., Donahue, N. M., and Robinson, A. L.:
675 Absorptivity of brown carbon in fresh and photo-chemically aged biomass-burning emissions, *Atmos. Chem. Phys.*, 13,
676 7683-7693, 10.5194/acp-13-7683-2013, 2013.
- 677 Saleh, R., Robinson, E. S., Tkacik, D. S., Ahern, A. T., Liu, S., Aiken, A. C., Sullivan, R. C., Presto, A. A., Dubey, M. K., Yokelson,
678 R. J., Donahue, N. M., and Robinson, A. L.: Brownness of organics in aerosols from biomass burning linked to their black
679 carbon content, *Nature Geoscience*, 7, 647, 10.1038/ngeo2220
680 <https://www.nature.com/articles/ngeo2220#supplementary-information>, 2014.
- 681 Saleh, R., Marks, M., Heo, J., Adams, P. J., Donahue, N. M., and Robinson, A. L.: Contribution of brown carbon and lensing
682 to the direct radiative effect of carbonaceous aerosols from biomass and biofuel burning emissions, *Journal of Geophysical*
683 *Research: Atmospheres*, 120, 2015JD023697, <https://doi.org/10.1002/2015JD023697>, 2015.
- 684 Saleh, R.: From Measurements to Models: Toward Accurate Representation of Brown Carbon in Climate Calculations, *Curr*



- 685 Pollut Rep, 6, 90-104, 10.1007/s40726-020-00139-3, 2020a.
- 686 Saleh, R.: From Measurements to Models: Toward Accurate Representation of Brown Carbon in Climate Calculations,
687 Current Pollution Reports, 10.1007/s40726-020-00139-3, 2020b.
- 688 Stier, P., Feichter, J., Kinne, S., Kloster, S., Vignati, E., Wilson, J., Ganzeveld, L., Tegen, I., Werner, M., Balkanski, Y., Schulz,
689 M., Boucher, O., Minikin, A., and Petzold, A.: The aerosol-climate model ECHAM5-HAM, Atmos. Chem. Phys., 5, 1125-
690 1156, 10.5194/acp-5-1125-2005, 2005.
- 691 Tao, J., Zhang, Z., Wu, Y., Zhang, L., Wu, Z., Cheng, P., Li, M., Chen, L., Zhang, R., and Cao, J.: Impact of particle number and
692 mass size distributions of major chemical components on particle mass scattering efficiency in urban Guangzhou in
693 southern China, Atmos. Chem. Phys., 19, 8471-8490, 10.5194/acp-19-8471-2019, 2019.
- 694 Tao, J., Surapipith, V., Han, Z., Prapamontol, T., Kawichai, S., Zhang, L., Zhang, Z., Wu, Y., Li, J., Li, J., Yang, Y., and Zhang, R.:
695 High mass absorption efficiency of carbonaceous aerosols during the biomass burning season in Chiang Mai of northern
696 Thailand, Atmospheric Environment, 240, 10.1016/j.atmosenv.2020.117821, 2020.
- 697 Wang, J. P., Nie, W., Cheng, Y. F., Shen, Y. C., Chi, X. G., Wang, J. D., Huang, X., Xie, Y. N., Sun, P., Xu, Z., Qi, X. M., Su, H., and
698 Ding, A. J.: Light absorption of brown carbon in eastern China based on 3-year multi-wavelength aerosol optical property
699 observations and an improved absorption Angstrom exponent segregation method, Atmospheric Chemistry and Physics,
700 18, 9061-9074, 10.5194/acp-18-9061-2018, 2018.
- 701 Wang, Q., Saturno, J., Chi, X., Walter, D., Lavric, J. V., Moran-Zuloaga, D., Ditas, F., Pöhlker, C., Brito, J., Carbone, S., Artaxo,
702 P., and Andreae, M. O.: Modeling investigation of light-absorbing aerosols in the Amazon Basin during the wet season,
703 Atmos. Chem. Phys., 16, 14775-14794, 10.5194/acp-16-14775-2016, 2016a.
- 704 Wang, X., Heald, C. L., Sedlacek, A. J., de Sa, S. S., Martin, S. T., Alexander, M. L., Watson, T. B., Aiken, A. C., Springston, S.
705 R., and Artaxo, P.: Deriving brown carbon from multiwavelength absorption measurements: method and application to
706 AERONET and Aethalometer observations, Atmospheric Chemistry and Physics, 16, 12733-12752, 10.5194/acp-16-12733-
707 2016, 2016b.
- 708 Wu, D., Mao, J., Deng, X., Tie, X., Zhang, Y., Zeng, L., Li, F., Tan, H., Bi, X., Huang, X., Chen, J., and Deng, T.: Black carbon
709 aerosols and their radiative properties in the Pearl River Delta region, Science in China Series D: Earth Sciences, 52, 1152-
710 1163, 10.1007/s11430-009-0115-y, 2009.
- 711 Yang, M., Howell, S. G., Zhuang, J., and Huebert, B. J.: Attribution of aerosol light absorption to black carbon, brown carbon,
712 and dust in China - interpretations of atmospheric measurements during EAST-AIRE, Atmospheric Chemistry and Physics,
713 9, 2035-2050, DOI 10.5194/acp-9-2035-2009, 2009.
- 714 Zhang, A., Wang, Y., Zhang, Y., Weber, R. J., Song, Y., Ke, Z., and Zou, Y.: Modeling the global radiative effect of brown
715 carbon: a potentially larger heating source in the tropical free troposphere than black carbon, Atmos. Chem. Phys., 20,
716 1901-1920, 10.5194/acp-20-1901-2020, 2020.
- 717 Zhang, G., Peng, L., Lian, X., Lin, Q., Bi, X., Chen, D., Li, M., Li, L., Wang, X., and Sheng, G.: An Improved Absorption Ångström
718 Exponent (AAE)-Based Method for Evaluating the Contribution of Light Absorption from Brown Carbon with a High-Time
719 Resolution, Aerosol and Air Quality Research, 19, 15-24, 10.4209/aaqr.2017.12.0566, 2019a.
- 720 Zhang, G. H., Peng, L., Lian, X. F., Lin, Q. H., Bi, X. H., Chen, D. H., Li, M., Li, L., Wang, X. M., and Sheng, G. Y.: An Improved
721 Absorption Angstrom Exponent (AAE)-Based Method for Evaluating the Contribution of Light Absorption from Brown
722 Carbon with a High-Time Resolution, Aerosol and Air Quality Research, 19, 15-24, 10.4209/aaqr.2017.12.0566, 2019b.
- 723 Zhao, G., Yu, Y., Tian, P., Li, J., Guo, S., and Zhao, C.: Evaluation and Correction of the Ambient Particle Spectral Light
724 Absorption Measured Using a Filter-based Aethalometer, Aerosol and Air Quality Research, 20, 1833-1841,
725 10.4209/aaqr.2019.10.0500, 2020.
- 726